Carbon 126 (2018) 183–189

Contents lists available at ScienceDirect

Carbon

journal homepage: www.elsevier.com/locate/carbon

Influence of dephasing and B/N doping on valley Seebeck effect in zigzag graphene nanoribbons

Lei Zhang [a, b, e], Zhizhou Yu [c, b], Fuming Xu [d], Jian Wang [b, *]

[a] State Key Laboratory of Quantum Optics and Quantum Optics Devices, Institute of Laser Spectroscopy, Shanxi University, Taiyuan, 030006, China
[b] Department of Physics and the Center of Theoretical and Computational Physics, The University of Hong Kong, Pokfulam Road, Hong Kong, China
[c] School of Physics and Technology, Nanjing Normal University, Nanjing, 210023, China
[d] College of Physics and Energy, Shenzhen University, Shenzhen, 518060, China
[e] Collaborative Innovation Center of Extreme Optics, Shanxi University, Taiyuan, 030006, China

ARTICLE INFO

Article history:
Received 13 July 2017
Received in revised form
29 September 2017
Accepted 6 October 2017
Available online 7 October 2017

ABSTRACT

We investigate the dephasing effect and atomic doping effect of random substitutional boron (B) or nitrogen (N) on the valley Seebeck effect in zigzag graphene nanoribbons (ZGNRs) using the tight-binding model calculations. When thermal gradient applied in the device made of ZGNRs is around several hundreds K, dephasing effect can only reduce the magnitude of pure valley current without generating electric current associated with the valley Seebeck effect. In the presence of B/N dopants, valley-polarized current occurs in ZGNRs. It is found that the generated valley polarized current is linearly dependent on the temperature gradient (ΔT) when the temperature of one lead is fixed and shows nonlinear dependence on temperature of a particular lead when ΔT is fixed. By calculating the phase diagrams such as $(\Delta T, p)$ with p the doping concentration, we find that the valley polarization can be tuned in a wide range from zero up to 0.72, indicating that it can be well controlled by B/N doping concentration. Finally, the noise power of valley Seebeck effect is also studied providing important information on the fluctuation of valley polarized current.

1. Introduction

In addition to charge and spin degrees of freedom, the manipulation and control of valley degrees of freedom of electrons attracted increasing attention in condensed matter physics community. In general, the valley index refers to the local maximum (minimum) of the valence (conduction) band in the first Brillouin zone [1–16]. As the potential information carrier, it can be utilized to store, manipulate and read out bits of information in the future electronics called valleytronics. Up to now, a variety of systems ranging from bulk to two dimensional materials have been proposed as potential building blocks of valleytronics, including silicon [1–3], bismuth [4], diamond [5], carbon nanotube [6], graphene [7–9,17], silicene [10], transition metal dichalcogenide monolayers (TMDs) [11–13,18–20], to just name a few. In particular, the successful isolation of 2D materials (such as graphene and TMDs) boost the rapid research advance in valleytronics. To achieve different functionalities in valleytronics, people proposed to use electric, magnetic, and optical means to manipulate and control the valley degree of freedom, which have been realized recently in experiment [11,18–20]. For instance, by applying the magnetic and optical field [11,20], the valley degeneracy in the system can be lifted and hence the valley polarized current can be generated and detected, which is extremely important for valleytronics.

Valleytronics may also find its application in caloritronics. Valley caloritronics [14–16], i.e., a combination of valleytronics and thermoelectrics, may provide an alternative way to harvest thermoelectric waste heat. Currently, the world energy consumption increases with an astonishing speed while huge amount of heat energy is wasted, which takes up a big portion in the energy loss. Therefore, the utilization of the heat waste becomes increasingly important. As a result, thermoelectricity has attracted great research attention in energy-saving technology [21,22]. Similar to spin caloritronics, the heat waste can also be used to induce the valley current in the absence of external bias voltage, which has great potential application in the future green energy technology. Indeed, the thermal means was recently proposed to generate the valley polarized current and as well as pure valley current without

* Corresponding author.
E-mail address: jianwang@hku.hk (J. Wang).

https://doi.org/10.1016/j.carbon.2017.10.017
0008-6223/

accompanying charge current [14–16]. As a result of a temperature gradient, the valley voltage difference across the system is generated which can drive the valley current in a valleytronic device. Since operation of valleytronic devices consume energy, in this sense, valley Seebeck effect can be used to harvest waste heat.

One of the important issues in valley caloritronics is to explore suitable materials for generation and manipulation of valley current using thermal means. In this work, we study the zigzag graphene nanoribbons (ZGNRs) for the following reasons. First of all, it has a very high melting temperature up to 4510 K and hence is thermally quite stable [23]. More importantly, two valleys in GNRs has a large separation in momentum space. The scattering due to the long wave length phonon between two valleys is small making the valley index a robust information carrier [8]. Note that our system involves temperature gradient so that the temperature in the central scattering region is not well defined at nanoscale. Since the temperature of leads are nonzero therefore there should exist phonons in the scattering region. However, since the temperature of the scattering region, where phonon is considered, is not well define, the relationship of the electron-phonon interaction and the temperatures of two leads will be very complicated. So rather than discussing this deep physics, we use a phenomenological theory in this paper, i.e., a dephasing mechanism to simulate the phonon, and use a parameter Γ_d to characterize the dephasing strength. In mesoscopic physics, it is known that the dephasing effect can have a large influence on quantum transport. For instance, dephasing effect can reduce the conductance when electron energy is near the resonance whereas an enhancement is observed in the case of off-resonance. It would be interesting to see what is the effect of dephasing on the valley current driven by thermal gradient. Furthermore, atomic doping in ZGNRs may provide another efficient way to tailor the electric transport properties of ZGNRs [24–30]. Therefore, it would be important to know whether doping effect can be used to modulate the valley Seebeck effect of ZGNRs and achieve different functionalities in valley caloritronics.

In this paper, we investigate the dephasing effect [31,32] and boron (B)/nitrogen (N) random atomic doping effect in the valley Seebeck effect of ZGNRs. It is found that by applying the temperature gradient across the device, the valley polarized current can be generated in the presence of B/N atomic doping. Furthermore, we find that the valley polarized current is linear with thermal gradient when the temperature of the right lead is fixed at 300 K. By increasing the doping concentration, the valley polarized current is decreasing while the electric current is increasing. Interestingly, the valley polarization can be effectively tuned by the doping concentration. This indicates that the doping mechanism can be used as an efficient tool in the application of ZGNRs in valley caloritronics.

2. Model and methods

In Fig. 1, a two terminal ZGNRs device with substitutional boron or nitrogen atomic dopants is shown. Here, B/N atomic dopants are randomly distributed in ZGNRs. In the tight-binding approximation of π orbitals, the Hamiltonian of ZGNRs can be expressed as

$$H = -t\sum_{\langle i,j\rangle}\left(c_i^\dagger c_j + c.c.\right) + \sum_{i\in d} V_i c_i^\dagger c_i, \tag{1}$$

where $c_i^\dagger$ (c_i) creates (annihilates) an electron on site i of ZGNRs. The first term of Eq. (1) represents the ideal ZGNRs with the nearest neighbor hopping energy t being 2.7 eV [33]. The second term of Eq. (1) describes the substitutional dopant with potential $V_i = 1.4$ or -1.4 eV for boron and nitrogen dopant located at site d, respectively [29]. In this study, we fix the size of ZGNRs device as $28.4\text{nm}\times 99.7\text{nm}$ and denote the doping concentration of B/N as p. Here we focus our attention to the zigzag graphene nanoribbon where the valley indices K and K' are well separated and well defined. While in the armchair graphene nanoribbon, K and K' points are mixed and hence is difficult to define two distinct valley indices. For the chiral nanoribbon, the distance between K and K is shorter than that in zigzag case. Therefore, the generation of valley polarized current due to the presence of B or N dopants should be larger than the case of zigzag for the same doping concentration.

In the framework of Landauer-Büttiker formula, the valley dependent current $I_{\alpha,\tau=K/K'}$ of αth lead driven by the temperature gradient $\Delta T = T_R - T_L$ can be written as

$$I_{\alpha,\tau} = \int\frac{dE}{2\pi}\sum_\beta\left(f_\alpha(E) - f_\beta(E)\right)\sum_{k\in\tau}\mathrm{Tr}\left[\widehat{T}^k_{\alpha\beta}(E)\right], \tag{2}$$

where $f_\alpha(E) = 1/(\exp[(E-E_F)/k_BT_\alpha]+1)$ denotes the Fermi-Dirac distribution of αth lead; E_F is the Fermi energy and T_α is the temperature in αth lead. In principle, the valley-resolved transmission operator $\widehat{T}^k_{\alpha\beta}(E)$ is defined as,

$$\widehat{T}^k_{\alpha\beta}(E) = \Gamma^k_\alpha G^r \Gamma_\beta G^a, \tag{3}$$

where $G^r = [G^a]^\dagger = [E - H - \sum_{\alpha=L,R}\Sigma^r_\alpha]^{-1}$ is the retarded and advanced Green's function, respectively. Here $\Gamma^k_\alpha = |W^k_\alpha\rangle\langle W^k_\alpha|$ is the linewidth function of αth lead with valley index τ and $|W^k_\alpha\rangle$ is eigenstate of $\Gamma_\alpha = i(\Sigma^r_\alpha - \Sigma^a_\alpha)$ with explicit momentum k [34–36]. Note that the traditional transmission coefficient $T_{\alpha\beta} = \sum_\tau\sum_{k\in\tau}\mathrm{Tr}[\widehat{T}^k_{\alpha\beta}(E)]$.

Therefore, the total valley and charge current $I_{\alpha,v/c}$ can be calculated by

$$\begin{aligned} I_{\alpha,v} &= I_{\alpha,K} - I_{\alpha,K'},\\ I_{\alpha,c} &= I_{\alpha,K} + I_{\alpha,K'}. \end{aligned} \tag{4}$$

To examine the valley current and its correlation, we note from the bandstructure of ZGNRs shown in Fig. 1(b) that the right moving electron is locked with valley K while the left moving electron is locked with valley K' in the first subband of ZGNRs. To characterize the valley polarization of current induced by the first subband, we introduce the following quantity

$$\eta = \frac{|I_{L,K}| - |I_{L,K'}|}{|I_{L,K}| + |I_{L,K'}|} = \frac{I_{L,c}}{I_{L,v}}. \tag{5}$$

Due to the discrete nature of quantum transport process, the electron transport is stochastic and hence the current usually fluctuates [37]. In order to obtain additional information about the fluctuations of valley current, it will be very interesting to study the noise power of valley resolved current [38].

$$S_\tau = \int\frac{dE}{2\pi}\sum_{k\in\tau}\mathrm{Tr}\left\{[(1-f_L)f_L + (1-f_R)f_R]\widehat{T}^k_{LR} + (f_L - f_R)^2\widehat{T}^k_{LR}\left(I - \widehat{T}^k_{LR}\right)\right\}, \tag{6}$$

and hence the noise power of total electric current.

In order to simulate the dephasing effect of e-ph, we adopt the Büttiker approach [31], which the fictitious voltage probes are introduced into the system to mimic the influence of phase-relaxing scattering. The Büttiker approach can be modeled by a self-energy term Σ^r_d [31,39–41].

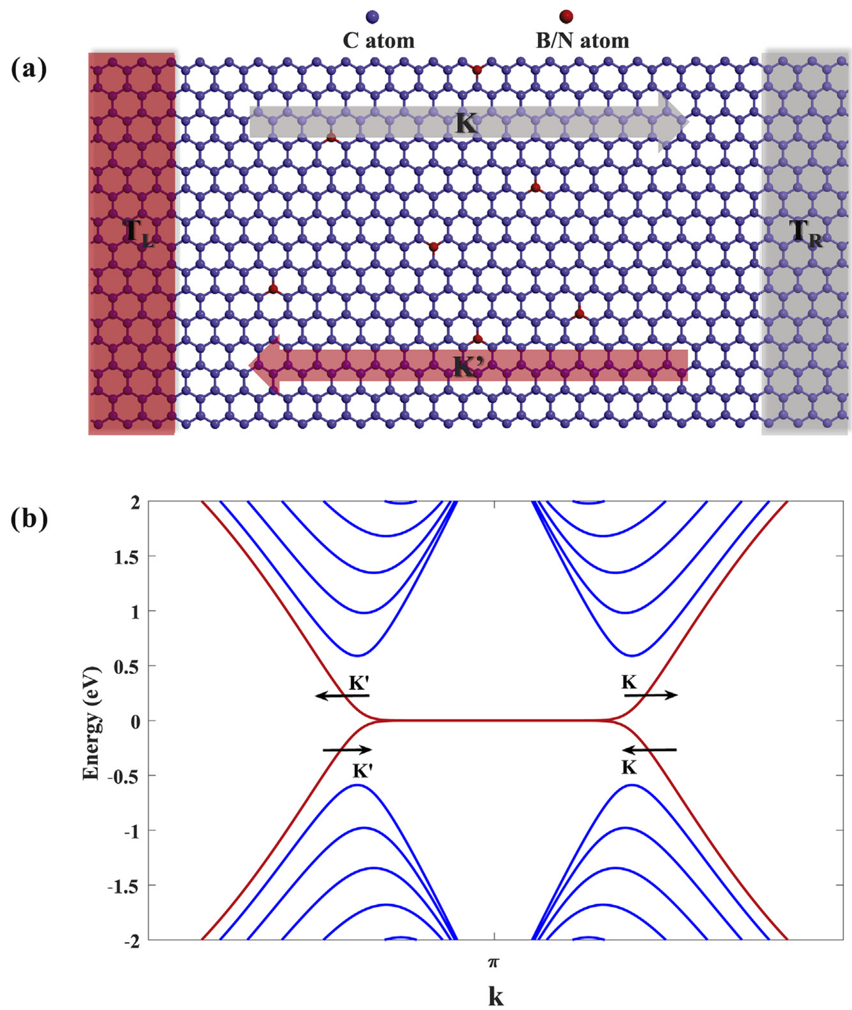

Fig. 1. (a). Schematic plot of a two-terminal ZGNRs device consisting of a central scattering region where substitutional B/N atoms are located, and left and right thermoelectrodes that has temperature difference ($\Delta T = T_R - T_L$). (b). Bandstructure of ZGNRs with 28.4 nm width. The index K and K' denotes two valleys and the arrow represents the moving direction of the electron. The first subbands are highlight with red color. (A colour version of this figure can be viewed online.)

$$\begin{aligned}\Sigma_d^r &= -i\frac{\Gamma_d}{2}I, \\ G_{ep}^r &= \left[E - H - \sum_{\alpha=L,R}\Sigma_\alpha^r - \Sigma_d^r\right]^{-1},\end{aligned} \tag{7}$$

where Γ_d denotes the dephasing strength. Here, the fictitious Büttiker probe is added to the each site of the system. Correspondingly, the current of any probe m can be expressed as

$$\begin{aligned}I_m &= \int\frac{dE}{2\pi}\sum_n(f_m(E) - f_n(E))T_{mn}(E), \\ T_{mn}(E) &= \mathrm{Tr}\left[\Gamma_m G_{ep}^r \Gamma_n G_{ep}^a\right],\end{aligned} \tag{8}$$

where $m, n \in [L, R, i]$ and i denotes the site of the system and $f_m(E) = f(E - \mu_m)$ is the Fermi Dirac distribution with chemical potential μ_m. To find the chemical potential of a particular fictitious probe, we require the current flowing into that probe to be zero. This gives N linear equations that determine μ_m, $(m = 1, 2, \ldots N)$ [40]. Finally, the valley resolved current in the presence of dephasing effect can be written as

$$I_{\alpha,\tau} = \int\frac{dE}{2\pi}\sum_n(f_\alpha(E) - f_n(E))\sum_{k\in\tau}\mathrm{Tr}\left[\hat{T}_{\alpha n}^k(E)\right], \tag{9}$$

where the transmission operator now is defined as $\hat{T}_{\alpha n}^k(E) = \Gamma_\alpha^k G_{ep}^r \Gamma_n G_{ep}^a$.

3. Results and discussion

Before analyzing the dephasing and atomic doping effect on valley Seebeck effect, we briefly discuss the electric and valley current in ZGNRs without any atomic dopants and dephasing mechanism. As shown in Fig. 1(b), the energy window of the first subband is $[-0.5, 0.5]$ eV, which corresponds to roughly 5800 K. In general, the applied thermal gradient in thermoelectrics is around a few hundreds K. Therefore, only electrons in the first subbands participate the transport process. When thermal gradient is applied in the pure ZGNRs, the difference of Fermi-Dirac function between two leads is an odd function of energy, i.e., $f_L(E) - f_R(E) = f_R(-E) - f_L(-E)$. More importantly, the transmission coefficient from the right lead to the left lead $T_{LR}^K(E<0)$ and $T_{LR}^{K'}(E>0)$ are exactly one for pure ZGNR without atomic dopants. As a result, the electric current of pure ZGNRs in the presence of thermal gradient is zero and a pure valley current is generated with zero valley polarization according to Eq. (5).

Now we discuss the influence of dephasing effect on the Valley Seebeck effect. Here the Büttiker dephasing scheme is adopted where the dephasing is modeled by a single parameter Γ_d. The parameter Γ_d can be considered as the average inelastic broadening parameter to describe the phase-relaxation effects. The numerical results of valley and electric currents for different values of the virtual probe dephasing parameter $\Gamma_d = 1$meV,25 meV in Fig. 2 (a) and (b). We see that the valley current $I_{L,v}$ shows a linear dependence on the temperature gradient ΔT (Fig. 2 (a)) when $\Gamma_d = 1$meV and deviates from the linear behavior when ΔT is large than 250 K and $\Gamma_d = 25$meV. While it is nearly independent of the temperature with fixed ΔT (Fig. 2 (b)) when dephasing effect is not considered. As we increase the dephasing strength Γ_d, the valley current $I_{L,v}$ decreases while the electric current $I_{L,c}$ remains to be zero. This is different from the dephasing effect on electric current due to bias voltage where the electric current $I_{L,c}$ or conductance is enhanced when dephasing strength is increased in the situation of off-resonance [31,40]. This indicates that the pure valley current is protected by the symmetry $T^K_{LR}(E) = T^{K'}_{LR}(-E)$ in the first subband of ZGNRs against the phase-relaxation caused by dephasing. As shown in Fig. 2 (a), we observe that the valley current $I_{L,v}$ has a larger decrease as increasing the temperature gradient ΔT when $\Gamma_d = 25$meV as compared to $\Gamma_d = 1$meV. When fixing ΔT we find that the suppression of valley current is more significant at low temperatures once the dephasing effect is on (see Fig. 2 (b)).

To generate a valley polarized current based on valley Seebeck effect, one has to break the symmetry $T^K_{LR}(E) = T^{K'}_{LR}(-E)$. In the following, we will show that this can easily be done by introducing B/N atomic dopants in the system. Fig. 3 presents the transmission in the clean system and averaged transmission $\langle T^{\tau}_{LR}\rangle$ versus the energy by considering several doping concentrations, i.e., $p = 3\%, 10\%$. Note that $\langle\ \rangle$ represents configuration average and ten thousand disorder configurations were used to calculate the average for each data. Here, we present the numerical results of

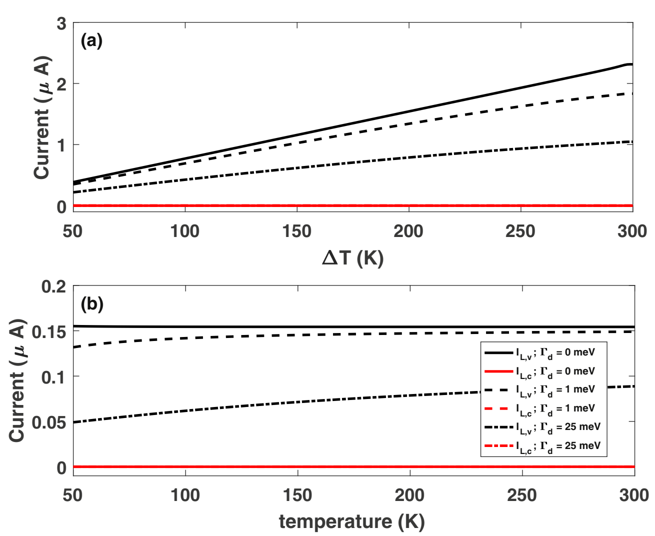

Fig. 2. (a) The valley (black lines) and electric (red lines) current versus the temperature gradient ΔT with the temperature of right lead being fixed at 300 K. (b) The valley (black lines) and electric (red lines) current versus the temperature with fixed $\Delta T = 20$ K. The electric current with or without considering dephasing effect (three curves in red) by are on top of each other. (A colour version of this figure can be viewed online.)

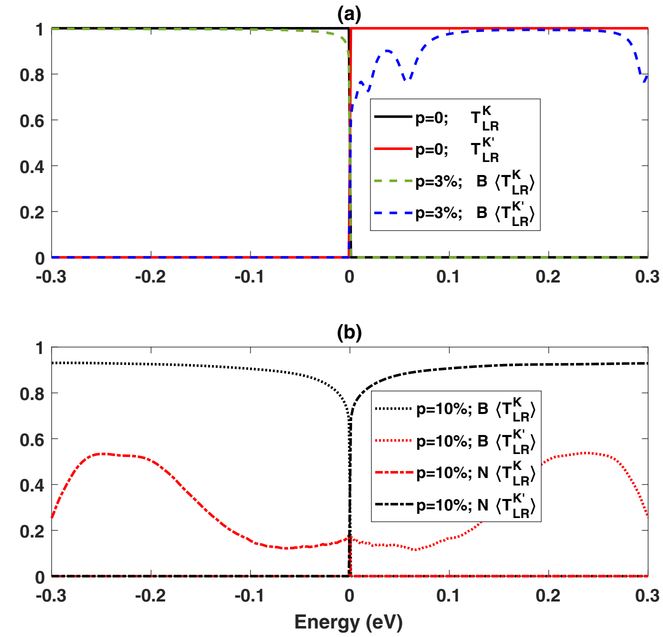

Fig. 3. (a). Pure and averaged transmission spectrum ($\langle T^{\tau}_{LR}\rangle$) of ZGNRs with $p = 3\%$ (b). Averaged transmission spectrum for $p = 10\%$ B and $p = 10\%$ N dopants. The black arrow indicates the transmission curves by increasing B doping concentrations. (A colour version of this figure can be viewed online.)

$\langle T^K_{LR}\rangle$ and $\langle T^{K'}_{LR}\rangle$. First of all, we see that the transmission $T^K_{LR}(E<0)$ and $T^{K'}_{LR}(E>0)$ are equal to one, while the transmission $T^K_{LR}(E>0)$ and $T^{K'}_{LR}(E<0)$ are equal to zero without any dopants shown in Fig. 3(a). Since the electrons injecting into the left lead are left moving, the corresponding electrons' momentum of left moving in the first subband with energy $E<0$ or $E>0$ are located in valley index K or K', respectively. The averaged transmission coefficient $\langle T^K_{LR}(E<0)\rangle$ for the first subband is much more robust than that $\langle T^{K'}_{LR}(E>0)\rangle$ for boron dopant. With increasing boron doping concentration, the averaged transmission coefficient $\langle T^{K'}_{LR}(E>0)\rangle$ decreases rapidly. For example, when doping concentration $p = 10\%$, the averaged transmission coefficient $\langle T^{K'}_{LR}(E=0.05)\rangle$ is nearly 0.1 while $\langle T^K_{LR}(E=-0.05)\rangle$ is equal to 0.9. Comparing with boron dopants, the effect of nitrogen dopants in ZGNRs is opposite in tuning the averaged transmission coefficient in the sense that $T^K_{B,LR}(E) = T^{K'}_{N,LR}(-E)$. As shown in Fig. 3 (b), the averaged transmission coefficient $\langle T^{K'}_{LR}(E>0)\rangle$ is robust against nitrogen doping and is sensitive to the doping for $\langle T^K_{LR}(E<0)\rangle$. Note that the averaged transmission coefficient $\langle T^K_{LR}(E<0)\rangle$ of boron dopants and $\langle T^{K'}_{LR}(E>0)\rangle$ of nitrogen dopants are symmetrical about $E = 0$ since the Hamiltonian in Eq. (1) is symmetrical with respective to energy with boron or nitrogen dopants. Thus, in the rest of paper we shall discuss the doping effect of B dopants only and the effect of N doping is immediately known.

Having understood the doping effect of B/N atoms on transmission coefficient in the ZGNRs, we now analyze how the valley current and electric current are controlled by doping effect in Fig. 4 (a). Here, we fix the temperature of the right lead as 300 K and plot valley/electric current versus the temperature gradient ($\Delta T = T_R - T_L$). It is found that the electric current is no longer zero and depend linearly on the temperature gradient when boron atoms are doped in the system. As we increase the doping concentration, the electric current is increasing which is unexpected.

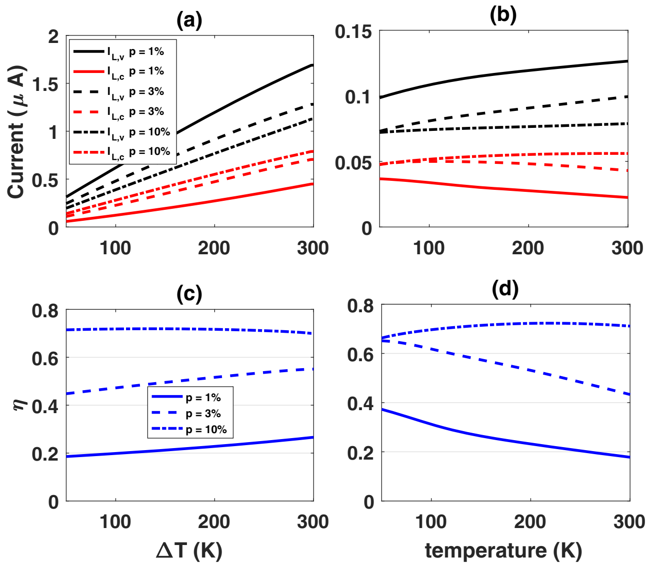

Fig. 4. (a) The valley (black lines) and electric (red lines) current versus the temperature gradient with the temperature of right lead being fixed at 300 K. (b) The valley (black lines) and electric (red lines) current versus the temperature with fixed $\Delta T = 20$ K. (c), (d) The corresponding valley polarization (blue lines) of different doping concentration versus the temperature gradient and temperature, respectively. Here solid, dashed, dashed dot lines correspond with $p = 1\%, 3\%, 10\%$, respectively. (A colour version of this figure can be viewed online.)

This is due to the following reason. The current is given by energy integration of $(f_L - f_R)\langle T^k_{LR}(E)\rangle$ where $k \in K, K'$ corresponding to two valleys. Since the Fermi energy is fixed at the Dirac point, i.e., $E_F = 0$, the current can be expressed as $\int dE\left(\langle T^K_{LR}(E<0)\rangle - \langle T^{K'}_{LR}(E>0)\rangle\right)$. As can be seen from Fig. 3, $\langle T^K_{LR}(E<0)\rangle$ is very robust against the atomic doping while $\langle T^{K'}_{LR}(E>0)\rangle$ decreases quickly as the doping concentration increases. This gives rise the counter-intuitive result, the increasing of current as we increase the doping concentration. The differential thermoelectric conductance dI/dT is about 1.8 nA/K for $p = 1\%$. Moreover, the dependence of valley current versus the temperature gradient is also linear but with larger slope. In contrast to the electric current, the magnitude of valley current decreases when the doping concentration is increasing. According to the definition of valley polarization η in Eq. (5), we present the numerical results in Fig. 4 (c). The valley polarization increases gradually with temperature gradient when doping concentration p is equal to 1% and 3%. For a rather large doping concentration 10%, the valley polarization is nearly a constant and equals to 0.72 from 50 K to 200 K. However, the valley polarization starts to drop slightly if the temperature gradient is increased further from 200 K to 300 K.

Furthermore, we also calculate the electric and valley current by fixing the temperature gradient ΔT while changing the temperatures of both leads. In the following, the calculated quantities are disorder averaged and $\langle\ \rangle$ will be ignored for simplicity. As shown in Fig. 4(b), the averaged valley and electric current show the nonlinear dependence on the temperature of the left lead with $\Delta T = 20$ K. For the doping concentration $p = 1\%$, the averaged electric current decreases as the temperature increases. At the same time, the averaged valley current is increasing over the whole temperature range. However, the electric current increases slightly and saturates at 50 nA when $p = 10\%$. In this case, the electric/valley current also increases/decreases with increasing of doping concentration. More importantly, the averaged valley polarization decreases when $p = 1, 3\%$ in Fig. 4 (d). For the doping concentration $p = 10\%$, the averaged valley polarization first increases and then decreases slightly. Thus, by fixing the temperature gradient or temperature of one lead, one can manipulate the valley polarization by doping mechanism.

To demonstrate the feature of the doping effect on valley polarization in a wide range of doping concentration, we have calculated the phase diagram for valley polarization η in Fig. 5. In the numerical calculations, each data point is averaged over three thousand configurations. Fig. 5(a) and (b) plot the valley polarization in the $(\Delta T, p)$ and (T, p) plane, respectively. For the entire range of ΔT, the valley polarization can be tuned from zero to 0.72 by increasing the doping concentration. Comparing with fixed temperature gradient, the phase diagram (T, p) plane shows that there is a large phase space (yellow region) where valley polarization roughly reaches a plateau ($\eta = 0.72$). Note that the nitrogen doping

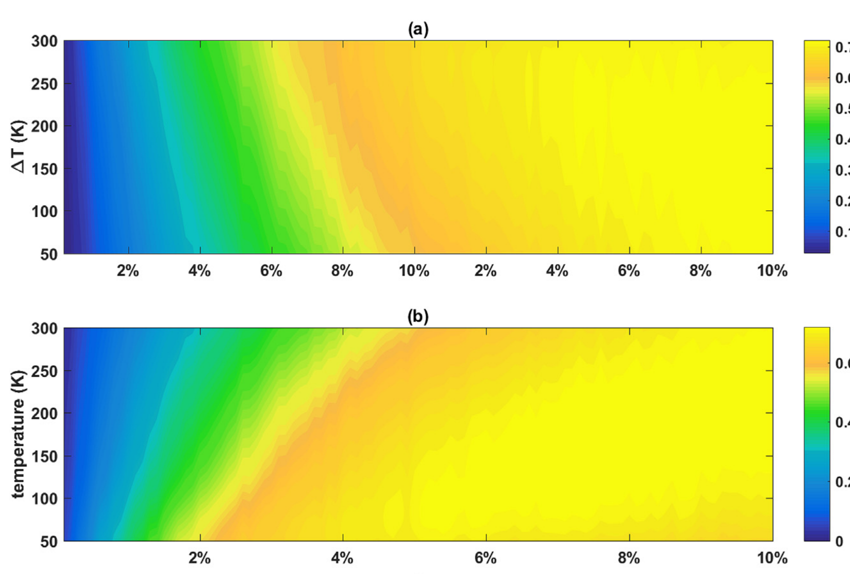

Fig. 5. Calculated phase diagram of valley polarization in the $(\Delta T(K), p)$ plane for the upper panel (a) and (T, p) plane for the lower panel (b). Three thousand configurations are calculated and averaged for each point on these phase diagrams. (A colour version of this figure can be viewed online.)

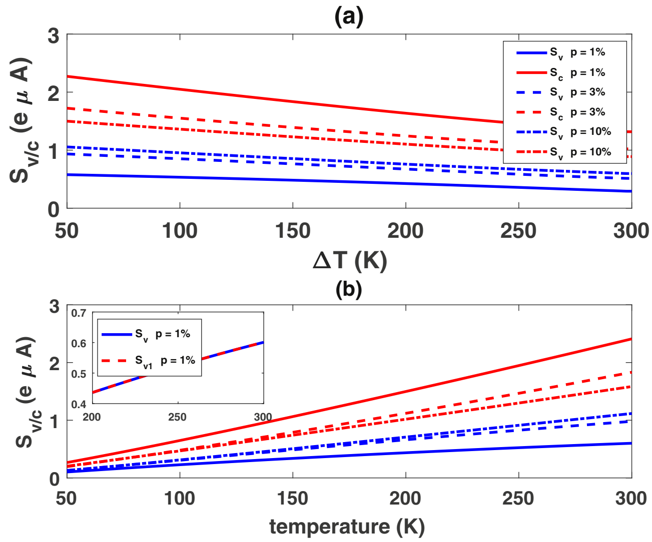

Fig. 6. (a) The noise power of valley and charge current versus the temperature gradient with the temperature of right lead being fixed at 300 K. (b) The noise power of valley and charge current versus the temperature with fixed $\Delta T = 20$ K. The insert figure presents the noise power S_v and the first term of noise power S_{v1} when $p = 1\%$. Here solid, dashed, dashed dot lines correspond with 1%, 3% and 10% doping concentrations, respectively. (A colour version of this figure can be viewed online.)

effect is expected to be opposite to that of boron dopants. Therefore, the valley polarization can also yield negative values, which indicates the electron with valley index K' can dominate the transport process. Therefore, the B/N doping effect can provide a rather wide range to tune the valley polarization of ZGNRs.

Last but not the least, we examine the fluctuations of generated valley polarized current by studying the noise power. The corresponding noise power of valley and charge current $S_{v,c}$ are shown in Fig. 6. It is interesting that the noise power is linear dependent on temperature for both cases, i.e., fixed temperature in one lead and temperature gradient. Moreover, the noise power of electric current is larger than that of the corresponding valley current. In the insets of Fig. 6 (b), we show the noise power of valley current I_v and its first term I_{v1} in Eq. (6) when $p = 1\%$. By analyzing the data, we find that the first term in Eq. (6) dominates. Since the second term is the second order in Fermi distribution, which is quite small comparing with the first term.

Finally, we note that the valley Seebeck effect is expected to exist in the system when the second-nearest neighbor hopping interaction is considered due to the broken of electron-hole symmetry [42–44]. If the bandgap of graphene nanoribbon shows up in the presence of antiferromagnetic order, there will be no valley Seebeck effect when the temperatures of both electrodes are within the energy gap. However, if the temperature of one lead is outside of the bandgap, the electric and valley current can be nonzero and but is smaller than that of the non-ferromagnetic order case. This is because the bandgap can result in tunneling effect that reduce the electric and valley current generated by the Seebeck effect.

4. Conclusion

In summary, we have investigated the effects of dephasing and random doping of boron and nitrogen atoms on valley Seebeck effect in ZGNRs. The results show that the pure valley current generated by the valley Seebeck effect is protected by the symmetry $T^K_{LR}(E) = T^{K'}_{LR}(-E)$ regardless of dephasing mechanism. While in the presence of random boron or nitrogen dopants which breaks the symmetry $T^K_{LR}(E) = T^{K'}_{LR}(-E)$, valley polarized current emerges. The generated valley polarized current is linearly dependent on temperature gradient when the temperature of one lead is fixed. Furthermore, the valley polarization of can also be effectively tuned in a wide range (from 0 to 0.72) by the doping concentration. According to our theoretical analysis, we find that the B/N doping mechanism in ZGNRs can be extremely useful in its potential application in valley caloritronics.

Acknowledgments

This work was financially supported by the National Natural Science Foundation of China (Grant No. 11704232, 11374246, 11504240, 11704190), the Research Grant Council (Grant No. 17311116), the University Grants Commission (Contract No. AoE/P-04/08) of the Government of HKSAR, Shanxi Science and Technology Department (No. 201701D121003).

References

[1] D. Culcer, A. Saraiva, B. Koiller, X. Hu, S.D. Sarma, Valley-based noise-resistant quantum computation using si quantum dots, Phys. Rev. Lett. 108 (12) (2012) 126804.
[2] K. Takashina, Y. Ono, A. Fujiwara, Y. Takahashi, Y. Hirayama, Valley polarization in si (100) at zero magnetic field, Phys. Rev. Lett. 96 (23) (2006) 236801.
[3] C. Yang, A. Rossi, R. Ruskov, N. Lai, F. Mohiyaddin, S. Lee, C. Tahan, G. Klimeck, A. Morello, A. Dzurak, Spin-valley lifetimes in a silicon quantum dot with tunable valley splitting, Nat. Commun. 4 (2013) 2069.
[4] O. Gunawan, Y. Shkolnikov, K. Vakili, T. Gokmen, E. De Poortere, M. Shayegan, Valley susceptibility of an interacting two-dimensional electron system, Phys. Rev. Lett. 97 (18) (2006) 186404.
[5] J. Isberg, M. Gabrysch, J. Hammersberg, S. Majdi, K.K. Kovi, D.J. Twitchen, Generation, transport and detection of valley-polarized electrons in diamond, Nat. Mater 12 (8) (2013) 760–764.
[6] A. Pályi, G. Burkard, Disorder-mediated electron valley resonance in carbon nanotube quantum dots, Phys. Rev. Lett. 106 (8) (2011) 086801.
[7] A. Rycerz, J. Tworzydło, C. Beenakker, Valley filter and valley valve in graphene, Nat. Phys. 3 (3) (2007) 172–175.
[8] D. Xiao, G.-B. Liu, W. Feng, X. Xu, W. Yao, Coupled spin and valley physics in monolayers of mos_2 and other group-vi dichalcogenides, Phys. Rev. Lett. 108 (19) (2012) 196802.
[9] D. Gunlycke, C.T. White, Graphene valley filter using a line defect, Phys. Rev. Lett. 106 (13) (2011) 136806.
[10] M. Ezawa, Spin valleytronics in silicene: quantum spin hall–quantum anomalous hall insulators and single-valley semimetals, Phys. Rev. B 87 (15) (2013) 155415.
[11] H. Zeng, J. Dai, W. Yao, D. Xiao, X. Cui, Valley polarization in mos_2 monolayers by optical pumping, Nat. Nanotechnol. 7 (8) (2012) 490–493.
[12] T. Cao, G. Wang, W. Han, H. Ye, C. Zhu, J. Shi, Q. Niu, P. Tan, E. Wang, B. Liu, et al., Valley-selective circular dichroism of monolayer molybdenum disulphide, Nat. Commun. 3 (2012) 887.
[13] L. Zhang, K. Gong, J. Chen, L. Liu, Y. Zhu, D. Xiao, H. Guo, Generation and transport of valley-polarized current in transition-metal dichalcogenides, Phys. Rev. B 90 (19) (2014) 195428.
[14] Z. Yu, F. Xu, J. Wang, Valley seebeck effect in gate tunable zigzag graphene nanoribbons, Carbon 99 (2016) 451–455.
[15] X. Chen, L. Zhang, H. Guo, Valley caloritronics and its realization by graphene nanoribbons, Phys. Rev. B 92 (15) (2015) 155427.
[16] X. Zhai, W. Gao, X. Cai, D. Fan, Z. Yang, L. Meng, Spin-valley caloritronics in silicene near room temperature, Phys. Rev. B 94 (24) (2016) 245405.
[17] F. Xu, Z. Yu, Y. Ren, B. Wang, Y. Wei, Z. Qiao, Transmission spectra and valley processing of graphene and carbon nanotube superlattices with inter-valley coupling, New J. Phys. 18 (11) (2016) 113011.
[18] S. Wu, J.S. Ross, G.-B. Liu, G. Aivazian, A. Jones, Z. Fei, W. Zhu, D. Xiao, W. Yao, D. Cobden, et al., Electrical tuning of valley magnetic moment through symmetry control in bilayer mos_2, Nat. Phys. 9 (3) (2013) 149–153.
[19] X. Xu, W. Yao, D. Xiao, T.F. Heinz, Spin and pseudospins in layered transition metal dichalcogenides, Nat. Phys. 10 (5) (2014) 343–350.
[20] D. MacNeill, C. Heikes, K.F. Mak, Z. Anderson, A. Kormányos, V. Zólyomi, J. Park, D.C. Ralph, Breaking of valley degeneracy by magnetic field in monolayer mose 2, Phys. Rev. Lett. 114 (3) (2015) 037401.
[21] F.J. DiSalvo, Thermoelectric cooling and power generation, Science 285 (5428) (1999) 703–706.
[22] B.C. Sales, Smaller is cooler, Science 295 (5558) (2002) 1248–1249.
[23] J. Los, K. Zakharchenko, M. Katsnelson, A. Fasolino, Melting temperature of graphene, Phys. Rev. B 91 (4) (2015) 045415.
[24] S. Kawai, S. Saito, S. Osumi, S. Yamaguchi, A. S. Foster, P. Spijker, E. Meyer, Atomically controlled substitutional boron-doping of graphene nanoribbons,

Nat. Commun. 6.
[25] B. Biel, X. Blase, F. Triozon, S. Roche, Anomalous doping effects on charge transport in graphene nanoribbons, Phys. Rev. Lett. 102 (9) (2009) 096803.
[26] P. Hirunsit, M. Liangruksa, P. Khanchaitit, Electronic structures and quantum capacitance of monolayer and multilayer graphenes influenced by al, b, n and p doping, and monovacancy: theoretical study, Carbon 108 (2016) 7–20.
[27] T. Aktor, A.-P. Jauho, S.R. Power, Electronic transport in graphene nanoribbons with sublattice-asymmetric doping, Phys. Rev. B 93 (3) (2016) 035446.
[28] T. Schiros, D. Nordlund, L. Palova, L. Zhao, M. Levendorf, C. Jaye, D. Reichman, J. Park, M. Hybertsen, A. Pasupathy, Atomistic interrogation of b–n co-dopant structures and their electronic effects in graphene, ACS Nano 10 (7) (2016) 6574–6584.
[29] S.-T. Pi, K.-P. Dou, C.-S. Tang, C.-C. Kaun, Site-dependent doping effects on quantum transport in zigzag graphene nanoribbons, Carbon 94 (2015) 196–201.
[30] X. Fei, J. Neilson, Y. Li, V. Lopez, S. J. Garrett, L. Gan, H.-J. Gao, L. Gao, Controlled synthesis of nitrogen-doped graphene on ruthenium from azafullerene, Nano Lett..
[31] M. Büttiker, Role of quantum coherence in series resistors, Phys. Rev. B 33 (5) (1986) 3020.
[32] R. Golizadeh-Mojarad, S. Datta, Nonequilibrium greens function based models for dephasing in quantum transport, Phys. Rev. B 75 (8) (2007) 081301.
[33] A.C. Neto, F. Guinea, N.M. Peres, K.S. Novoselov, A.K. Geim, The electronic properties of graphene, Rev. Mod. Phys. 81 (1) (2009) 109.
[34] J. Wang, H. Guo, Relation between nonequilibrium greens function and lippmann-schwinger formalism in the first-principles quantum transport theory, Phys. Rev. B 79 (4) (2009) 045119.
[35] P. Khomyakov, G. Brocks, V. Karpan, M. Zwierzycki, P. Kelly, Conductance calculations for quantum wires and interfaces: mode matching and greens functions, Phys. Rev. B 72 (3) (2005) 035450.
[36] L. Zhang, Y. Xing, J. Wang, First-principles investigation of transient dynamics of molecular devices, Phys. Rev. B 86 (15) (2012) 155438.
[37] Y.M. Blanter, M. Büttiker, Shot noise in mesoscopic conductors, Phys. Rep. 336 (1) (2000) 1–166.
[38] Y. Wei, B. Wang, J. Wang, H. Guo, Nonlinear voltage dependence of shot noise, Phys. Rev. B 60 (24) (1999) 16900.
[39] H. Jiang, S. Cheng, Q.-F. Sun, X. Xie, Topological insulator: a new quantized spin hall resistance robust to dephasing, Phys. Rev. Lett. 103 (3) (2009) 036803.
[40] J. Maassen, F. Zahid, H. Guo, Effects of dephasing in molecular transport junctions using atomistic first principles, Phys. Rev. B 80 (12) (2009) 125423.
[41] Y. Xing, Q.-F. Sun, J. Wang, Influence of dephasing on the quantum hall effect and the spin hall effect, Phys. Rev. B 77 (11) (2008) 115346.
[42] Y. Yao, F. Ye, X.-L. Qi, S.-C. Zhang, Z. Fang, Spin-orbit gap of graphene: first-principles calculations, Phys. Rev. B 75 (4) (2007) 041401.
[43] Y.-W. Son, M.L. Cohen, S.G. Louie, Energy gaps in graphene nanoribbons, Phys. Rev. Lett. 97 (21) (2006) 216803.
[44] S. Young-Woo, M.L. Cohen, S.G. Louie, Half-metallic graphene nanoribbons, Nature 446 (7133) (2007) 342.